DOI: 10.1007/s10297-005-0050-4
Originally published in J. Opt. Fiber. Commun. Rep. 2, 530–557 (2005)

New optical device technologies for ultrafast OTDM systems

T. Sakurai[1] and N. Kobayashi[2]

[1] Photonics Research Institute (PRI)
National Institute of Advanced Industrial Science and Technology (AIST)
1-1-1 Umezono, Tsukuba, Ibaraki 305-8568 Japan
Email: teruo-sakurai@aist.go.jp
[2] National Institute of Advanced Industrial Science and Yechnology (AIST)
1-1-1 Umezono, Tsukuba, Ibaraki 305-8568 Japan
Email: naoto.kobayashi@aist.go.jp

Abstract. Optoelectronic devices handling high bit-rate signals of picosecond or sub-picosecond pulse repetitions are necessary for the OTDM or OTDM/WDM-mixed systems. The bit-rate is 1st or 2nd order higher than the operation speed of conventional devices. To meet the higher speed requirement, we have to develop ultrafast optoelectronic device technologies in new device principles and materials.

1. Introduction

A national project of the Femtosecond Technology (FST project) in Japan that is sponsored by NEDO (New Energy and Industrial Technology Development Organization) develops ultrafast optoelectronic devices in order to make OTDM/WDM-mixed Tb/s-class photonic networks possible. The project was started in 1995 and will reach its goal in 2004. FESTA (The Femtosecond Technology Research Association) and AIST (National Institute of Advanced Industrial Science and Technology) execute the project in cooperative works.

Most of the optoelectronic devices are based on the semiconductor device and material technology in the project. We also develop organic dye aggregates as new materials for the ultrafast optical switch. The reason why we challenge these devices and materials instead of fiber-based technologies is the stable operation and the possibility of device integration in future.

One of the key issues is the generation and the formation of ultrashort light-pulses in the signal transmission. Mode-locked semiconductor laser diodes are suitable for

oscillators of light pulses and/or standard signal pulses in OTDM light sources due to their low jitter characteristics (see section 2). The group-velocity-dispersion compensation is one of big issues in the ultrashort-pulse laser and in the OTDM transmission. We developed a semiconductor pulse compressing device and a pulse shaping device respectively for the dispersion compensation [1]. Pulse compressing devices are composed of the semiconductor coupled-waveguide structure and will be used to make the chirped laser-pulse width short in transmitters. Fiber Bragg gratings will be applied to adaptive pulse forming devices for compensating pulse form fluctuations by the environmental temperature in the long haul transmission [2].

Optical switches as optical node devices in the OTDM/WDM-mixed system will be operated above 160 Gb/s. Speed limits of current electronic technologies are believed to be about 100 Gb/s and the optical switches must be operated by some other control pulses than electronic ones. Light pulses are used for the purpose. These devices are called as all-optical switches.

Ultrafast optical switches developed in the project are based on new phenomena and/or new materials. SMZ (Symmetric Mach-Zehnder) switches composed of PLC (Planar Lightwave Circuit) Mach-Zehnder interferometer and SOAs for phase modulation were used in the Demux and logic operations (see section 3). The PLC will be replaced with photonic crystal waveguides in future. The photonic crystal SMZ device partially embedded with quantum dots as optical nonlinear materials, i.e., PC-SMZ, is expected to have abilities of small size and device integration. The ISBT (Inter Subband Transition) switch uses high-speed recovery characteristics of the absorption saturation in the quantum wells (see section 4). Ultrafast optical gates and Demux are its promising applications. The two-photon resonance multi-layer device utilizing the Kerr effect enhanced by the optical field confinement will be used as an ultrafast optical gate [3].

FESLAP (Femtosecond Large Area Parallel Processor) switches using the saturation absorption in organic dye aggregates convert the time serial signals to space parallel signals (see section 5). This switch is suited for header recognition in photonic nodes because of dividing the frequency for lower-frequency circuit operations. The high-speed wavelength conversion at the node is required in the OTDM/WDM-mixed system. Four-wave mixing in semiconductor gain medium is employed in wavelength conversion devices (see section 6).

Precise characterization of light pulses is inevitable for the development of optical devices. Timing jitter measurements were developed using time domain methods of both the time domain demodulation and the time interval analysis. For high repetition rate OTDM pulses, new technologies of the double-balanced mixing and the optoelectronic harmonic mixing were combined to these time domain methods (see section 7). The ultrashort light-pulses are extremely chirped and broadened under chromatic dispersion in optical fibers because of their broadband spectrum. Time-dependent variation of the pulse waveform is significant in long-distance propagation due to variation of chromatic dispersion under temperature drift. We have developed a frequency-resolved optical gating method using two-photon absorption, which enables high-sensitivity real-time characterisation in time-spectral domain of the pulses [4].

In this paper, we will introduce several ultrafast optical devices developed in the Femtosecond Technology Project.

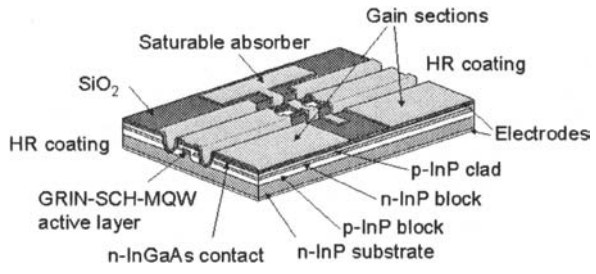

Fig. 1. Schematic structure of CPM-LD.

2. Mode-Locked Laser Diodes

Ultrafast optical pulse generation is of great interests for many applications, such as optical time division multiplexing systems, soliton transmission systems, optical measurement systems, and so on. Mode-locked laser diodes (MLLD) are very attractive for such applications because of its small size, high reliability, and high stability. Furthermore, a passively mode-locked laser diode (PML-LD) has the fascinating feature of generating ultrafast optical pulses beyond limit of electrical speed, because it needs no external modulation source for pulse generation [5]. In practical use, the most important technical problems of PML-LD are synchronization of such high repetition pulses to an external clock signal and reduction of the comparably large timing jitter. Hybrid mode-locking [6] and optical synchronous mode-locking are well-known methods for stabilization of PML-LD. These methods, however, require an electrical/optical signal with a repetition frequency almost equal to that of the PML-LD. In this section, the generation of ultrafast optical pulse train with a mode-locked laser diode and its control techniques are described.

Figure 1 shows a schematic structure of a colliding-pulse mode-locked laser diode (CPM-LD) [7]. The CPM-LD is a kind of PML-LDs in which the saturable absorber is placed at the center of the laser cavity. Both the gain and the absorber sections consist of eight compressively strained InGaAsP quantum wells separated by In-GaAsP barriers, with the GRIN-SCH for avoiding the electrical screening effect by trapped photo-carriers at hetero-interface. The mode-locking frequency can be basically increased as the cavity length is shortened. However the mode-locking frequency is restricted by the carrier dynamics in the saturable absorber. When the repetition time is close to or beyond the recovery time of the saturable absorber, the modulation depth at the saturable absorber become shallow. And then, the pulse width becomes broader and the mode-locking operation itself is impeded in the worst case. This is because the GRIN-SCH structure is introduced to the high repetition MLLD. When the currents were injected to the two gain sections and the absorber section was reverse biased suitably, passive mode-locking occurred. Figure 2 shows (a) SHG correlation trace and (b) optical spectrum of the output of the CPM-LD. The saturable absorber section was 17 μm and the total cavity length was about 174 μm. The repetition frequency was about 480 GHz, which coincided with twice the round-trip frequency estimated

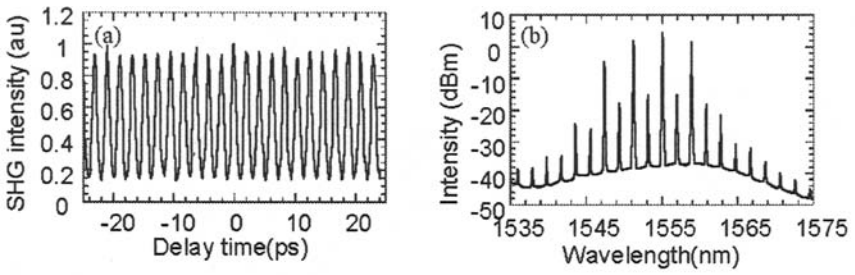

Fig. 2. (a) Correlation trace and (b) optical spectrum of CPM-LD with the cavity length of 174 μm.

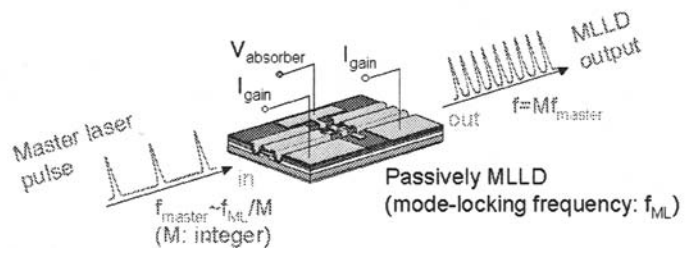

Fig. 3. SSML method.

from the cavity length. The pulse width was estimated to be 0.58 ps, assuming the sech^2 waveform. The center wavelength and the spectral width were 1555 nm and 8 nm, respectively. The time-bandwidth product was 0.58, close to the transform limited value of sech^2 pulses.

When the mode-locking frequency is extremely high, subharmonic optical synchronous mode-locking (SSML) [8,9] by a subharmonic frequency optical pulse injection (Fig. 3) is the most promising way for synchronization with an external signal because this can be achieved with low-frequency master laser pulses and the application is not limited by bandwidth of the drive electronics. The 480-GHz CPM-LD has been stabilized by the SSML, using the hybrid mode-locked laser diode as a master laser. The repetition frequency of the master laser (f_{master}) was 9.954 GHz, corresponding to 48th subharmonics of the slave laser's repetition frequency (f_{ML}). The center wavelength and the pulse width were about 1558 nm and 1.6 ps, respectively. In the SSML experiment, no significant degradations were observed in both of the pulse shape and the optical spectrum when the injected power was below -10 dBm.

Figure 4 shows an experimental setup for the jitter measurement of ultrafast optical pulses [10]. Ultrafast optical pulses with frequency of f_{ML} and reference pulses with frequency of f_{ref} were injected in a semiconductor optical amplifier (SOA) simultaneously. Beat signal was generated due to nonlinear coupling for cross gain modulation

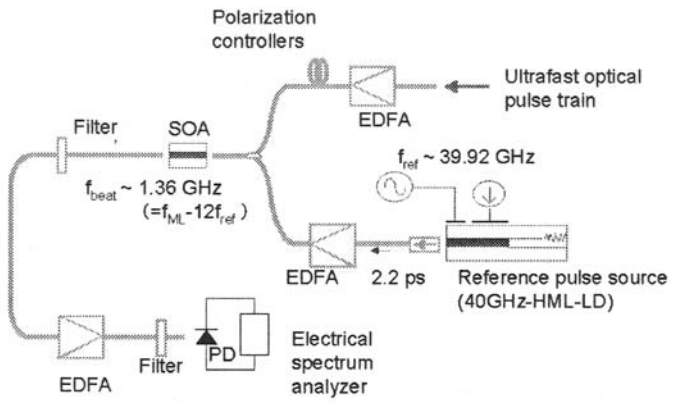

Fig. 4. Experimental setup for the timing jitter measurements of 480 GHz CPM-LD.

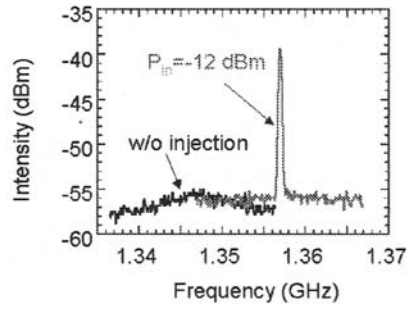

Fig. 5. Changes in electrical power spectra of beat signals in the SSML of 480 GHz CPM-LD.

between those pulses. We can estimate the timing jitter of the ultrafast optical pulse train from the SSB noise of the beat signal, because the squared timing jitter of the beat signal is given by the summation of those of the signal and the reference pulse trains. In this experiment, the reference pulse source was a hybrid mode-locked laser diode. The repetition frequency of the reference pulse train was 39.919 GHz. The pulse width, the center wavelength, and the timing jitter were 2.25 ps, 1539.5 nm, and 0.23 ps, respectively. Figure 5 shows the changes in the beat power spectra with and without the master laser pulse injection. Without master laser pulse injection, the spectrum was broadened and no discrete frequency component was observed. This indicates that the mode-locking frequency fluctuated under the passive mode-locking operation. In contrast, a discrete frequency component corresponding to $f_{\mathrm{ML}} - 12 f_{\mathrm{ref}}$ appeared and the side band noise level decreased with master laser pulse injection at the average power of -12 dBm. This implies that the mode-locking frequency of the CPM-LD was exactly locked to 48th harmonics of the master laser's repetition frequency and

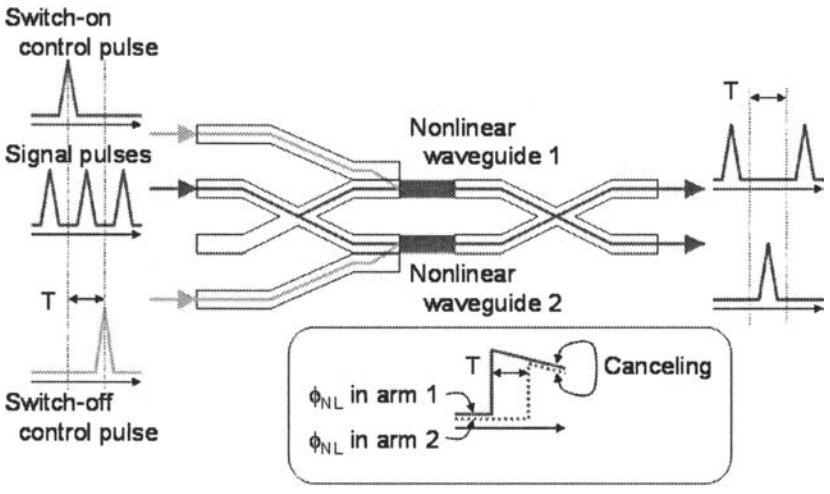

Fig. 6. Schematic representation of a symmetric Mach-Zehnder all-optical switch. Differential phase modulation is also illustrated in the inset.

that the timing jitter was also reduced. The timing jitter was estimated to be about 0.14 ps, less than that of the master laser. Stable ultrafast optical pulse generation by SSML is very promising as a compact and reliable pulse source for future advanced applications.

3. Symmetric Mach-Zehnder Type All-Optical Switches and Ultrafast All-Optical Signal Processing

3.1. Symmetric Mach-Zehnder (SMZ) Type All-Optical Switches

A symmetric Mach-Zehnder (SMZ)-type ultra-fast all-optical switch has been developed for a key device in an optical-time-division-multiplexing (OTDM) system [11,12]. From practical application point of view, one of the requirements for all-optical switches is that a control-light-pulse energy must be much less than 1 pJ, otherwise the control light power is too high even at a few tens of Gb/s. To satisfy this requirement, the SMZ switch uses semiconductor optical amplifiers (SOAs) for nonlinear elements to enhance the band-filling non-linearity in semiconductors by stimulated emission. This enables true femto-joule switching, but the relaxation time of SOAs limits the operating speed to less than a few tens of Gb/s. A promising way to mitigate this problem is to use a differential phase modulation (DPM) scheme [11]. In this way, the difference in nonlinear phase shifts (ϕ_{NL}) optically induced in the two nonlinear elements defines the state of the switch, so the effect of slow relaxation is circumvented, as illustrated in Fig. 6. The DPM scheme also realizes a rectangle-like switching window, which is highly desirable in many applications. There are two

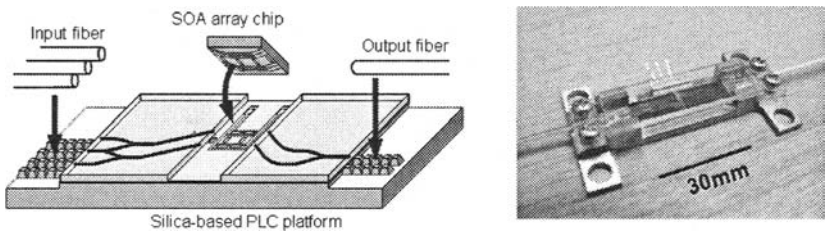

Fig. 7. Structure and photograph of a hybrid-integrated symmetric Mach-Zehnder all-optical switch.

variants of the SMZ switch: a polarization-discriminating SMZ [13] (PD-SMZ, often called UNI) and a delayed-interference signal-wavelength converter (DISC) [14]. These devices can be configured in inherently stable forms suitable for bulk optics implementation. The original SMZ switch, on the other hand, can be unstable unless integrated. Hybrid-integrated [15,16] (Fig. 7) and monolithic [17] SMZ-type switches have been reported.

3.2. Ultra-Fast All-Optical Signal Processing With the SMZ All-Optical Switches

As an example of ultra-fast all-optical signal processing, a de-multiplexing experiment is explained here, in which the original 42-Gb/s signal is retrieved (de-multiplexed) from a 336-Gb/s signal that is made by optically time-division-multiplexing 8–42 Gb/s signal channels. Figure 8 shows an experimental setup. A HI (hybrid integrated)-SMZ all-optical switch is driven by a 42-GHz control pulse train to retrieve 42 Gb/s signal pulses from 336 Gb/s signal pulses. Control pulses were generated by multiplexing the output of a mode-locked fiber laser (MLFL, 10.5 GHz) twice by two-stage optical delay lines. The 336 Gb/s signal was generated from the same MLFL. Here the output of the MLFL was compressed, wavelength converted, and modulated with a pseudo-random bit sequence (PRBS) of 2^7-1 before being multiplexed to 336 Gb/s by optical delay lines. The low noise compression and wavelength conversion were achieved by first generating super-continuum in an optical fiber, spectrally slicing it by a filter, and applying a dispersion compensating technique. In this experiment, the control pulse width was set relatively wide (1.5 ps), compared with the interval (3.0 ps) and the width (0.9 ps) of the 336 Gb/s signal pulses, to minimize the degradation in switching characteristics due to the intra-band effects in the SOA type nonlinear phase shifters. If the control pulse width approaches or exceeds 1 ps, the switching energy increases and the differential phase modulation becomes less complete, because of the hole burning and the subsequent carrier heating effects in SOAs [18]. Of course, wider control pulses allow a higher level of crosstalk between adjacent bits, but it is a weak function of the control pulse width, because of the sinusoidal transfer function characteristic of a Mach-Zehnder interferometer. Thus, the degradation in switching characteristics and the cross-talk are compromised at 1.5 ps. Figure 9(a) shows an eye-diagram of the 336 Gb/s input signal measured by an optical sampling oscilloscope, indicating uniformity

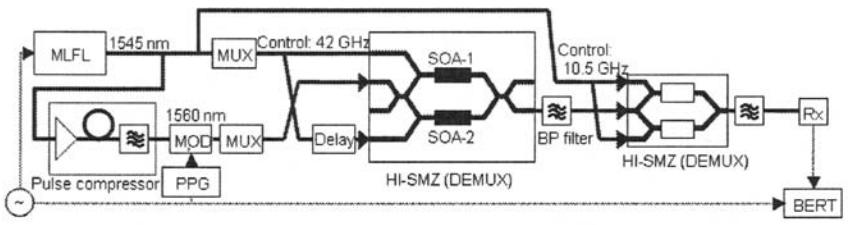

Fig. 8. Setup for 336→42 de-multiplexing experiment. MOD: EO optical modulator, PPG: Pulse-pattern generator, Rx: Receiver system, BERT: Bit-error-rate tester.

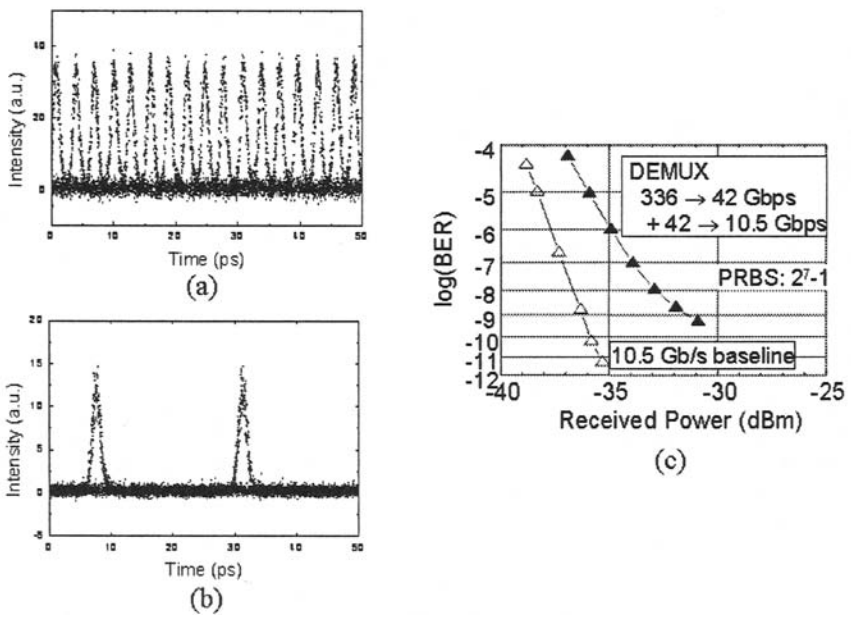

Fig. 9. (a) Eye-diagram of the 336-Gb/s input signal. (b) Eye-diagram of the 42-Gb/s signal de-multiplexed from the 336-Gb/s input signal. (c) Result of bit-error-rate measurements of 336→42 Gb/s de-multiplexing (42→10.5 Gb/s optical de-multiplexing).

in multiplexing from 10.5 to 336 Gb/s, while Fig. 9(b) shows an eye-diagram of the de-multiplexed 10.5 Gb/s signal. The extinction ratio between de-multiplexed and rejected pulses was approximately 17 dB. A bit-error-rate (BER) was assessed at 10.5 Gb/s after further de-multiplexing the output 42 Gb/s pulses down to 10.5 Gb/s signal by using another HI-SMZ. As can be see from Fig. 9(c), error free operation (BER $< 10^{-9}$) was achieved.

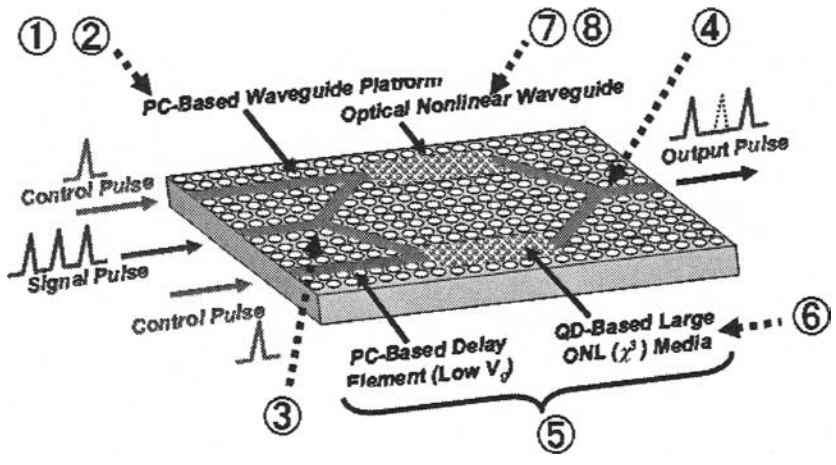

Fig. 10. Schematic diagram of a 2DPC slab waveguide-based all-optical switch (PC-SMZ).

3.3. Challenging Photonic Crystal-Based Ultra-Small All-Optical Switches

A GaAs two-dimensional photonic crystal (2DPC)-based ultra-small symmetrical Mach-Zehnder (SMZ) all-optical switch (hereafter referred to as PC-SMZ) was proposed [19]. 2DPC straight- [20], bent- [21], Y-branch- [22], directional coupler- [23], quantum dot (QD)-embedded nonlinear-waveguides [24] and a PC-SMZ chip including these waveguides [25] have been fabricated using a GaAs air-bridge membrane with triangular-lattice line-defect waveguides. Figure 10 shows a schematic picture of the PC-SMZ. Technical key issues are indicated by numbers 1–8. InAs quantum dots (QDs) as optical nonliear (ONL) mateials are embedded only in the straight ONL phase-shift arms between the Y-branch splitter (3) and Y-junction coupler (4). The device is expected to exhibit optical switching at a speed of over 40 Gb/s on a principle of the conventional SMZ switch, while optical switching energy can be dramatically reduced by using a low group velocity (V_g), appearing in the vicinity of a photonic bandgap [24,26].

So far, single chip of the PC-SMZ was integrated in the area of about 500 $\times$ 500 μm^2 [25], while an extremely low propagation loss, less than 1 dB/mm, obtained recently [27,28] allows us to integrate many chips in the area up to 1 cm in length. For the Y-junction (4), use of a directional coupler [23] instead of a three-fold symmetry Y-branch enables exhibiting a desired SMZ interference, otherwise an undesirable ring resonance mode is generated in the SMZ loop. In the QD-embedded ONL arm, on the other hand, a phase shift $\Delta\phi$ of $\pi/2$, which is necessary for operation of the SMZ switching, was verified experimentally [29], while enhancement of the ONL effect by use of the low V_g was predicted theoretically [24].

Typical SEM (canning electron microscope) photographs and transmittance spectra of the PC-SMZ membrane are shown in Fig. 11 [25]. Figure 11(a)–(c) show a total

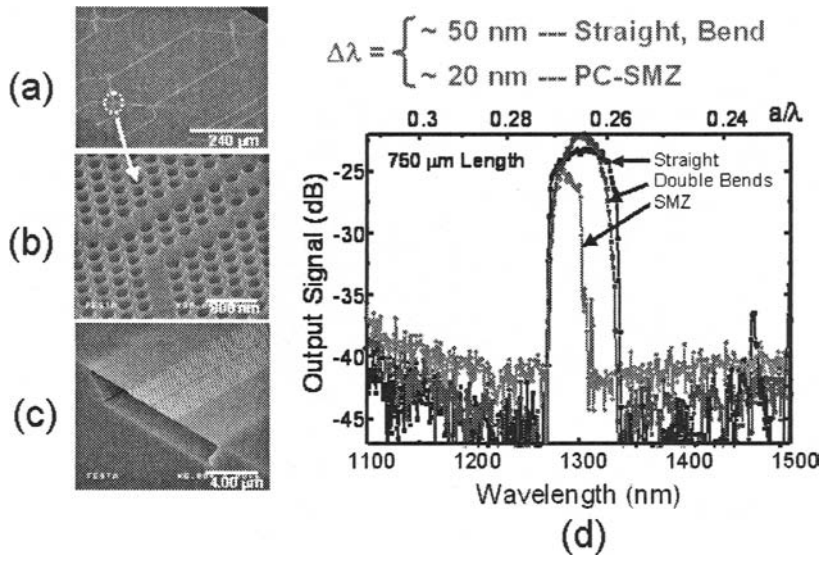

Fig. 11. (a)–(c): SEM photographs of an air-bridge type 2DPC slab waveguide sample including PC-SMZ patterns. (d) Transmittance spectra of the PC-SMZ membrane.

PC-SMZ pattern, expanded part of the directional coupler and cleaved edge of the air-bridge, respectively, while Figure 11(d) shows transmission spectra of straight, double bend and PC-SMZ-waveguides. A bandwidth of the PC-SMZ is narrower (~20 nm) than those of the straight and bend waveguides (~50 nm). Nevertheless, it should be noted that the transmittance of the PC-SMZ is not so degraded as that of the straight waveguide, taking into account that the PC-SMZ involves eight bends between the input and output ports.

3.4. Conclusion

A symmetric Mach-Zehnder (SMZ) all-optical switch achieves ultra-fast, low-power switching by differential phase modulation. So far, ultra-fast de-multiplexing from 336 to 10.5 Gb/s was performed. The application of this device is not limited to de-multiplexing alone. Error-free all-optical regeneration at 84 Gb/s [30] and error-free wavelength conversion at 168 Gb/s [31] have also been reported, indicating the high repetition capability of SMZ type all-optical switches. On the other hand, a 2DPC-based GaAs ultra-small SMZ all-optical switch was also developed. Air-bridge membranes including the PC-SMZ pattern as well as straight, bend, Y-branch and directional coupler waveguides were fabricated and characterized in the 1.1–1.55 μm wavelength region. 2DPC technologies developed here is promising not only for the PC-SMZ but also for wide applications to other ultra-small photonic integrated circuits.

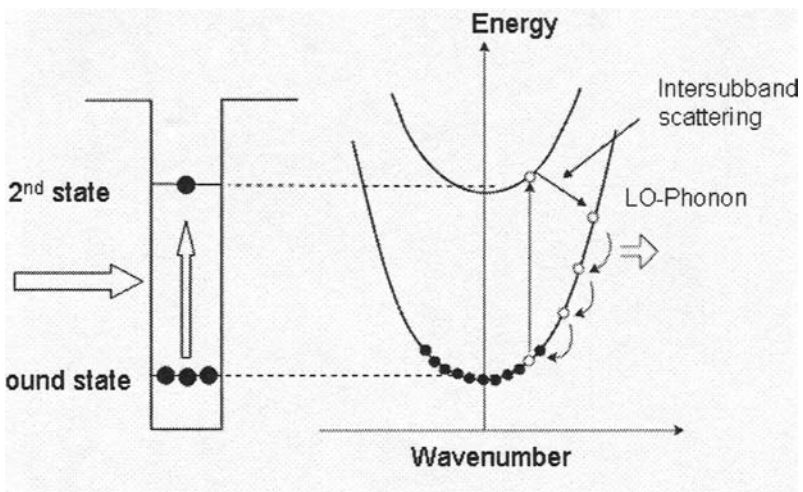

Fig. 12. Schematic potential lineup and subband structure of quantum well.

4. Ultrafast All-Optical Switch Using Intersubband Transition in Quantum Well

4.1. Introduction

Absorption saturation effect in the intersubband transition (ISBT) of a quantum well is very attractive for ultrafast all-optical switches because of its very fast absorption recovery [32]. Since it is necessary to use deep potential well to obtain 1.55 μm-intersubband transitions, we are investigating three types of material systems. The investigation will also provide us deeper understanding of ISBT leading to the development of better performance switches. Here, we first review the principle of the ISBT switch and show the-state-of-the-art development.

4.2. Principle of the ISBT Switch

Figure 12 shows the potential lineup and the corresponding band diagram of a quantum well. The well layer is heavily doped and then the ground state is occupied by electrons. If we illuminate the quantum well with an intense p-polarized optical pulse (gate pulse) whose wavelength corresponds to the transition wavelength between the ground state and the second state, the carriers in the ground state is excited to the second state. When the carrier number in the ground state and the upper sate becomes equal, the quantum well is transparent. Therefore a small intensity signal pulse can transmit through the quantum well; it means that the switch is in the "on" state. After the excitation pulse, carriers in the second state relax to the ground sate and then the quantum well is absorptive again, i.e., the switch is in the "off" sate. The most attractive feature of the ISBT is that the excited carriers relax to the ground state with a time constant of a few

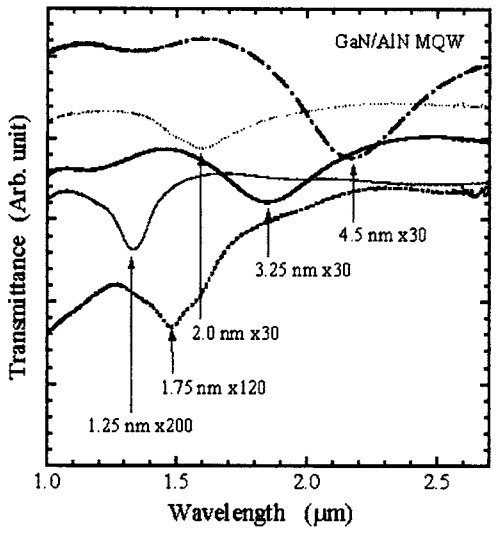

Fig. 13. Transmittance of GaN/AlN quantum well for various well layer thicknesses and layer numbers.

100 fs to a few ps. Because of this very fast relaxation time, we can make use of ISBT for ultrafast all-optical switches.

To realize intersubband transition at the communication wavelength of 1.55 μm, we need a very deep potential well. Three material systems are being developed. They are GaN/AlGaN system [33–37] (well depth; 2 eV), InGaAs/AlAsSb system [38–40] (1.6–1.7 eV), and CdS/ZnSe/BeTe system [41,42] (2.3 eV). Even with these materials we need a very thin quantum well of a thickness of a few mono-layers to obtain the transition wavelength of 1.55 μm.

The absorption recovery time is mainly limited by intersubband scattering time. The scattering time depends on electron effective mass, dielectric constant, and LO-phonon energy [43]. The calculated scattering times are 90 fs in GaN, 2500 fs in InGaAs, and 180 fs in CdS. The scattering time is the shortest in GaN and the longest in InGaAs.

4.3. Quantum Wells for ISBT

4.3.1. GaN/AlGaN Quantum Well

The fastest response speed can be expected with this material because of the shortest intersubband scattering time. We started the growth of GaN/AlGaN quantum well using MOCVD and attained very fast response speed of 150 fs at the wavelength of 4.5 μm [34]. However, it was difficult to obtain the absorption peak at shorter wavelengths of below 2.9 μm. We therefore changed the growth method to MBE and changed the barrier layer to AlN [35]. Figure 13 shows the absorption spectrum for various well layer thicknesses and numbers. Barrier thickness was 4.5 nm. A high density doping of

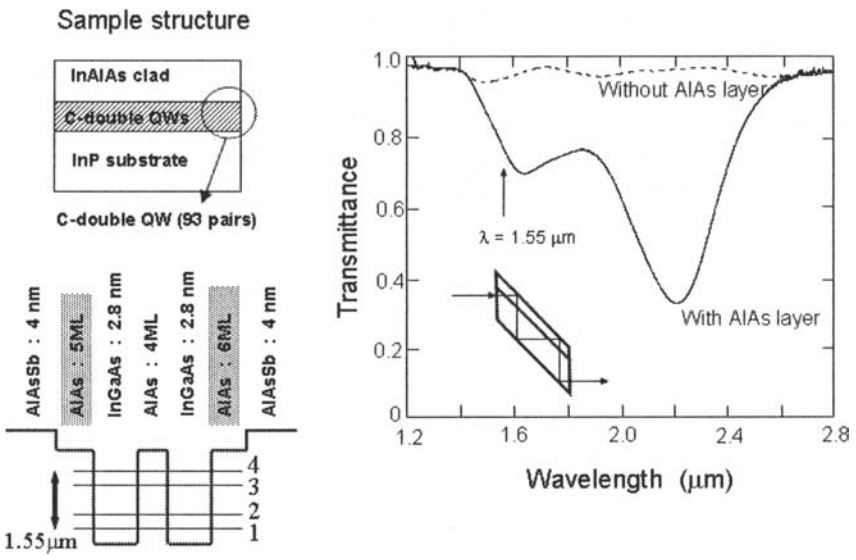

Fig. 14. (a) Sample structure and the potential lineup. (b) Transmittance of the coupled-double quantum well. Light was introduced at the 45 degrees lapped wafer end. Multiple reflections were used.

8×10^{19} cm^{-3} was performed to the well layer. In the measurement p-polarized light was injected to the grown quantum well in Brewster angle. The shortest absorption wavelength was 1.33 μm. The saturation energy, which is pulse energy to give half of the initial absorption coefficient, was measured to be 500 fJ/μm^2 at 1.55 μm. The response speed at this wavelength was estimated to be 400 fs.

4.3.2. InGaAs/AlAsSb Quantum Well

The potential well depth of this system is rather shallow than that of GaN/AlN and CdS/ZnSe/BeTe systems. It was then difficult to obtain the transition wavelength of 1.55 μm with InGaAs/AlAsSb single-quantum well due to the inter-diffusion of composite atoms between well and barrier layer. To suppress the inter-diffusion, we inserted a few mono-layers of AlAs between the InGaAs well layer and AlAsSb barrier layer [38]. Further we introduced a coupled-quantum well structure. Figure 14 shows the coupled-quantum well structure and the absorption spectrum [40]. The coupled-quantum well structure splits the ground state and upper state. We can obtain the transition wavelength of 1.55 μm between sublevels 1 and 4. The insertion of a few mono-layers of AlAs at the interface increased the absorption coefficient largely. Absorption spectrum without insertion of AlAs layer is also shown for comparison. It was also confirmed that the coupled quantum well gives faster response than the single quantum well [41]. This is because of the second sublevel serving as a carrier reservoir, which rapidly supplies carriers to the depleted ground state. We obtained absorption recovery time of 600fs in the coupled quantum well, while the time was 1.5–2.0 ps in

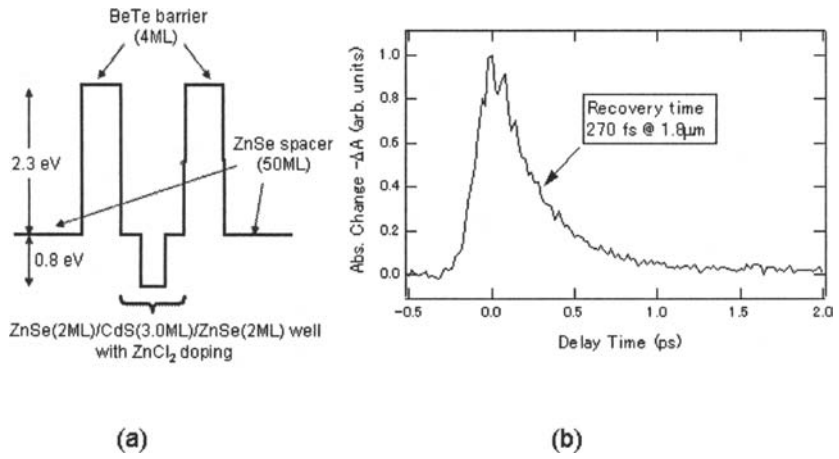

Fig. 15. (a) A schematic potential lineup of CdS/ZnSe/BeTe quantum well. (b) Absorption recovery under short pulse excitation.

the single quantum well. The absorption saturation of the quantum well was evaluated with the same measurement configuration as shown in the inset of Fig. 14. The value ranged 40 fJ/μm^2 to a several hundred fJ/μm^2.

4.3.3. CdS/ZnSe/BeTe Quantum Well

Figure 15(a) shows the structure of the quantum well. The well layer consists of very thin CdS layer and ZnSe layers [42]. The CdS layer was introduced to eliminate the effect of X-band in the BeTe cladding layer. The thin CdS layer lowers the energy levels so that the second level is lower than the X-band of the BeTe layer. This eliminates the carrier relaxation via X-band in BeTe layer, and enables us to obtain very fast response. Figure 15(b) shows the response for a sample whose absorption peak is 1.8 μm. We can confirm a very fast recovery of 270fs. The saturation powers ranging 100–600 fJ/μm^2 were obtained for the samples with absorption peak wavelength of 1.6–1.8 μm. The shortest absorption wavelength so far achieved with this quantum well was 1.58 μm.

4.4. ISBT Switching Device

Waveguide-type switching device is under development for these three types of material systems. Figure 16 shows an example of the device structure realized using InGaAs/AlAs/AlAsSb coupled-quantum well [39]. A ridge type waveguide is used and the ridge is tilted by about 7 degrees to reduce the reflection at the facet. Figure 16 shows the input pulse energy versus transmittance characteristics of the device for a pulse width of 150 fs. In this case 40 pairs of coupled-quantum well were used. Transmission increased by 3 dB for input-pulse energy of 20 pJ. The problem in this specific device is that the two-photon absorption is large as evidence in the steep reduction in

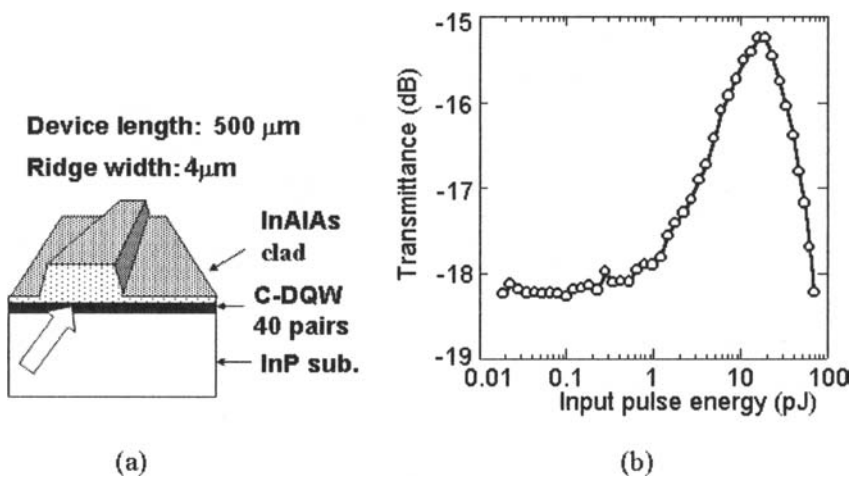

Fig. 16. (a) Schematic structure of ridge-waveguide type ISBT switch. (b) Transmittance of the ISBT switch for 150-fs gate pulse.

transmittance at high pulse energy. This two-photon absorption comes mainly from the InP substrate. The reduction of the field penetration to the substrate would improve this situation largely and the improved structure is under development.

4.5. Summary

Because of material parameters, the GaN, and CdS/ZnSe well layer gives very fast response while the InGaAs quantum well gives slower response. It is a general principle that higher energy is needed for faster response. Therefore it will be necessary to select material systems depending on the applications considering required switching speed and energy. One of the promising applications of the ISBT switch is ultrafast switching in OTDM systems. At present, the switching energy and the extinction of InGaAs/AlAsSb device are yet unsatisfactory. We can further improve the performances by employing the structure to reduce the two-photon absorption, and further reduction of the switching energy by the improvement of the quantum well. Devices using GaN/AlN, and CdS/ZnSe/BeTe quantum well are also under development to realize ultrafast switches.

5. All-Optical Spatial Switch Using Ultrafast Nonlinear-Optical Response of Organic Films

5.1. Introduction

In the field of optical switching materials, compound semiconductors such as InGaAs and dielectric materials such as silica optical fibers have been commonly used.

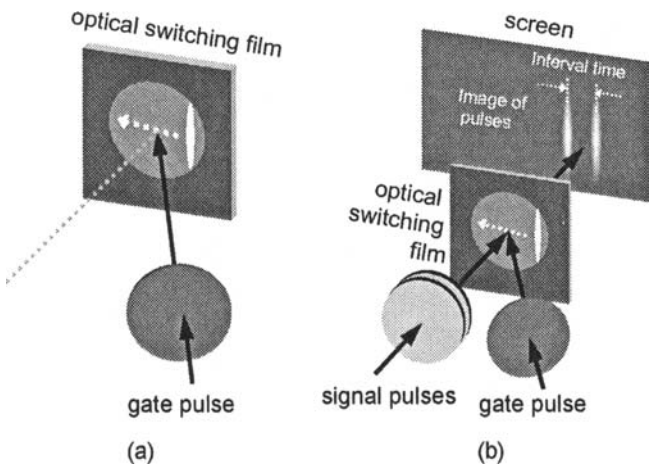

Fig. 17. Principle of ultrafast moving slit (a) and serial to parallel conversion of signal pulses (b) activated by irradiation of a gate pulse from horizontally oblique angle.

Semiconductors exhibit high nonlinear-optical susceptibility, however speeds of their responses are relatively slow. For silica fibers, ultrafast switching can be achieved while requires long interaction length because of lower susceptibility. To fabricate ultrafast all-optical switches using such materials, device structures should be designed to utilize their characteristics effectively. In case of organic dye molecules, strong absorption at resonant wavelength of $\pi - \pi^*$ transition reflects in exhibition of high nonlinear susceptibility. Furthermore, when highly ordered molecular arrangement called J-aggregates are formed, ultrafast decay of response can be achieved [44,45]. Characteristics of organic materials lie on strong interaction with the light at resonant wavelength and should be used in a form of thin film. In order to make full use of these ultrafast organic films, unique concepts of optical switches would be desired.

5.2. Principle of the FESLAP

Femtosecond laser pulses are characterized by short duration, strong peak intensity and thinness in propagation direction. A laser pulse of 100 fs duration has thinness of only 30 μm. A train of femtosecond laser pulses at 1 Tbit/s aligns with distance of 0.3 mm to each other. When keeping eyes on this thinness of the femtosecond pulses and an organic thin film exhibiting ultrafast response, we can observe a cross-sectional intensity distribution of pulses in space domain by using the film as an ultrafast shutter. As shown in Fig. 17(a), when activation gate pulse of a switching film irradiated in a horizontally oblique angle, only narrow intersection area of the film and the gate pulse turned to be transparent like a slit at a certain instant. The slit moves with propagation of the gate pulse, which acts as an ultrafast shutter. If we irradiate other signal pulses from normal direction to the film, a spatial patten of the signal pulses will be projected on a screen behind the film as shown in Fig. 17(b). The spatial distance between the

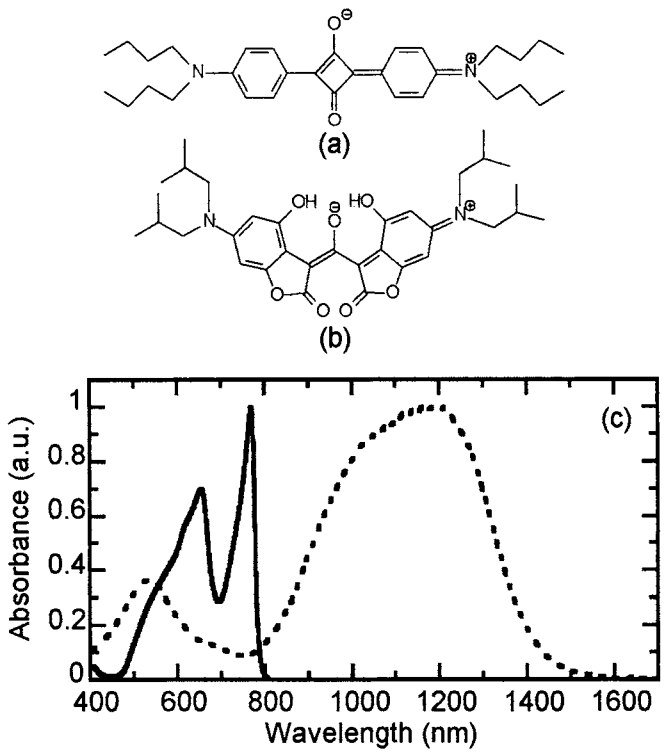

Fig. 18. Chemical formulas and absorption spectra of organic dye molecules for ultrafast optical switching; SQ (a) and solid line, BM (b) and broken line.

observed narrow lines on the screen indicates the interval time between the signal pulses. Using an ultrafast switching film, train of serial pulses in Tbit/s repetition rate can be converted into parallel pulses in space domain of mm size, which corresponding the light velocity. We named this principle to be FESLAP: femtosecond large-area parallel processor [46]. Although similar method for measuring time profiles of short pulses using converted spatial patterns of them have been proposed using second harmonic generation from a nonlinear crystal [47] and optical Kerr gate of quartz plate [48], our proposed principle has advantage in simplicity of the configuration, wider dynamic range and lower driving energy.

5.3. Verification of the Principle of FESLAP

For the materials of the ultrafast optical switching films, we have been studying on formation and characterization of squarylium-dye J-aggregates (SQ-J) film and reported that the SQ-J film exhibit ultrafast and efficient absorption saturation [49, 50]. We also succeeded synthesis of a new type of infrared absorbing dye molecules (BM dye), which exhibit ultrafast switching around telecommunication wavelength range [51]. Chemical formulas and absorption spectra of these dye molecules and films are shown

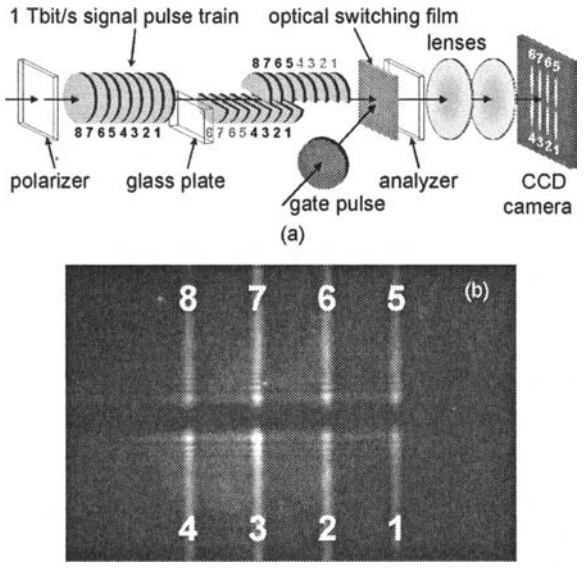

Fig. 19. Experimental set up for serial-to-parallel conversion of a 1-Tbit/s signal pulse train into two-dimensionally aligned pulses (a) and a typical image of converted signal pulses observed by a CCD camera (b).

in Fig. 18. In order to verify the principle of FESLAP, we used the SQ-J film for a switching film [52]. As shown in Fig. 19(a), we applied optical Kerr gate configuration to achieve enough on/off ratio. A train of 8 signal pulses with time interval of 1 ps is formed by splitting and joining fs laser pulses at 773 nm using half mirrors and retro-reflectors. Time delay of 4 ps is added to lower half of the signal pulse train passed though a polarizer using transparent glass plate. A single gate pulse at 810 nm with polarization 45 degrees tilted to the polarizer irradiates the SQ-J film in horizontally oblique angle with the signal pulses. Part of each pulse in the signal pulse train, which irradiate an area on the SQ-J film where the gate pulse irradiates in the same timing changes to tilted elliptically polarization because of instantaneously induced dichroism and birefringence by the gate pulse. Finally, different part of each pulse in the signal pulse train passes thorough cross-polarized analyzer. As the result, an image of two-dimensionally arranged signal pulses was observed on a charge coupled device (CCD) camera as shown in Fig. 19(b). Switching on/off ratios more than 5 were observed under gate pulse energy density of 2 pJ/ μm^2.

5.4. Future Prospects

We also think on the required efficiency of the switching for practical applications. Such open-air configuration requires irradiation of the gate pulse in large area on the film where switching of signal pulses occur only a small restricted area (or a spot). In order to reduce switching energy, it is effective that focusing signal and gate pulses to

the same small spots on the film. We can achieve the same driving energy densities with much lower total energy through tight focusing and reducing the size of switching spots. Further progress in configuration of this optical switch using focusing lenses and enlarging number of output channels through modularizations of optical components is now in progress.

6. Sub-Picosecond Wavelength Conversion by Four-Wave Mixing in Distributed-Feedback Laser and Semiconductor Optical Amplifiers

6.1. Introduction

High-speed wavelength conversion is strongly required in the future OTDM/WDM all optical network. In order to operate this network smoothly, the wavelength conversion occurs at every node.

The idea introduced here is to construct the simple wavelength conversion devices. We utilize the four wave mixing process (FWM). We try using two devices of the distributed feedback (DFB) laser and the semiconductor optical amplifiers (SOA). In the following the performance of these two types of wavelength conversion is introduced.

6.2. FWM With DFB Lasers

The FWM using lasers has been first proposed and demonstrated by H. Nakajima et al. [53]. In this report, the lasing light working as the pump is a conventional Fabry-Perot lasers. FWM using DFB lasers have been demonstrated in highly nondegenerate case [54] and in nearly degenerate case [55]. Wavelength conversion for input signals with continuous wavelengths has been demonstrated using a $\lambda/4$ phase shifted DFB laser [56].

To realize the wavelength conversion of short pulses with a pulsewidth of less than several pico-seconds, there are two subjects to be overcome; the suppression of a slow component of the 3rd order nonlinear effect and the avoidance of the cavity mode of a laser cavity.

$\lambda/4$ phase shifted DFB lasers are suitable for the overcome of these subjects [57]. The carrier density pulsation effect can be suppressed due to the stopband of the grating. In usual case, the carrier density effect strongly occurs in the small detuning of less than 100 GHz from the pump frequency and generates a long tail in converted pulses. In a $\lambda/4$ phase shifted DFB laser, the small detuning components in signal pulses and converted pulses are blocked by the stop-band. The cavity mode effect can be also avoided. A $\lambda/4$ phase shifted DFB laser has anti-reflection coatings in both facets. The laser works as the traveling wave semiconductor optical amplifier for the signal pulse and the converted pulse.

The structure of a $\lambda/4$ phase-shifted DFB laser used in the experiment of short pulse wavelength conversion is shown in Fig. 20. The auto-correlation traces of an input signal pulse of a wavelength of 1558 nm and an output converted pulse of a wavelength of 1548 nm are shown in Fig. 21. The pulsewidths are estimated to be 1.4 ps for input and 2.5 ps for output under the assumption of the hyperbolic cosine pulse shape. The result shows that a long tail of several 10 ps due to the carrier density pulsation effect is suppressed.

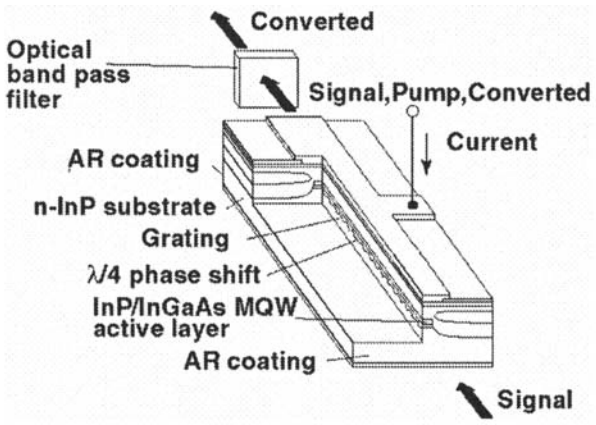

Fig. 20. The arrangement of wavelength conversion using FWM in a $\lambda/4$ phase shifted DFB laser. The signal pulse is input from one side of facets of the laser. The converted pulse is obtained from another side of the facets.

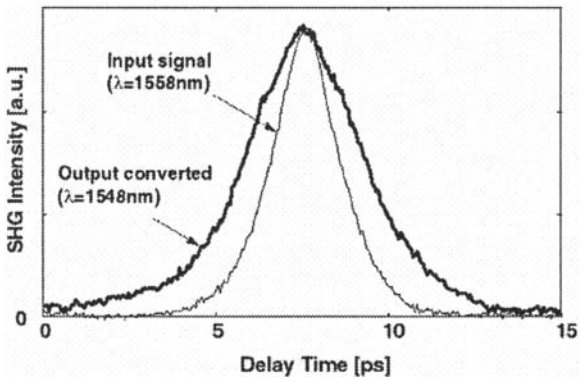

Fig. 21. The auto-correlation trace of a pulse after wavelength conversion. The peak wavelength of the pulse is converted to 10 nm shorter than that of the input signal pulse.

6.3. FWM With SOA

Conventional SOAs with the bulk or quantum-well active region have a drawback that the efficiency of the conversion to longer wavelengths is too small [58,59]. The application of quantum-dot SOAs to this scheme is attractive, because of the possibilities of eliminating destructive interference and obtaining symmetric, i.e., direction-independent, and large conversion efficiency by their small linewidth enhancement factor as well as their intense spectral hole burning [60]. The conversion efficiency is proportional to the absolute value of the third-order susceptibility given as

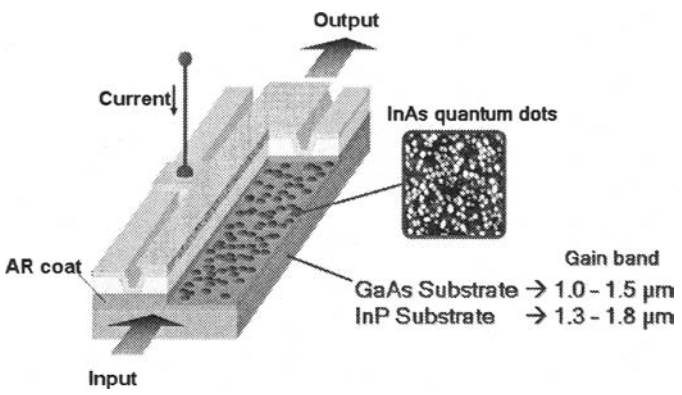

Fig. 22. Structure of the quantum-dot SOA, with self-assembled InAs quantum dots in the active region.

$$\chi^{(3)} = A_p \frac{\beta_p \Delta T_{\text{in}}}{\Gamma_{\text{cv}}[\Delta\omega^2 + T_{\text{in}}^2]} + \frac{\alpha\Delta\omega + (R_{\text{rec}} + R_{\text{stim}})}{[\Delta\omega^2 + (R_{\text{rec}} + R_{\text{stim}})^2]}, \tag{1}$$

where the first term on the right-hand side represents the contribution of the spectral hole burning, the second term is that of the carrier density pulsation, A_p is the differential gain, T_{in} is the intraband relaxation rate, $\beta_p \Delta$ is the constant inversely proportional to the differential gain, Γ_{cv} is the polarization dephasing rate, α is the alpha parameter, R_{rec} is the carrier recombination rate, R_{stim} is the stimulated emission rate, and $\Delta\omega = \omega_p - \omega_s$ is the detuning. Equation (1) tells us that the zero alpha parameter enables symmetric conversion and that the slower relaxation rate of $T_{\text{in}} = 200$–300 fs in quantum dots than that of $T_{\text{in}} = 10$–50 fs in conventional semiconductors improves efficiency.

Figure 22 shows the structure of the quantum-dot SOA, with self-assembled InAs quantum dots in the active region. With the inputs of both the pump at the frequency of ω_p and the signal lights at ω_s, we obtain the converted signal at $\omega_c = 2\omega_p - \omega_s$.

Figure 23 shows the conversion efficiency for positive (closed circles) and negative (open circles) detuning [61]. Remarkable differences were observed in comparison with those in a bulk SOA (taken from [58]); The efficiency for both the positive and negative detuning in the quantum-dot SOA has become almost same (symmetric). The detuning dependence is much flatter due to the spectral-hole burning. These results are indicative of the advantages of quantum-dot SOAs as devices for FWM wavelength conversion.

6.4. Summary

The FWM has the merit of fast wavelength conversion. We introduced two promising types. The introduced devices have merits and demerits in the present stage. We need the much improvement keeping each merit. These devices are key devices in the future all optical networks.

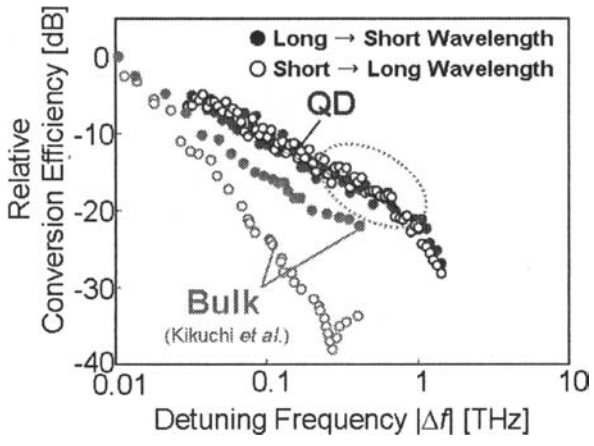

Fig. 23. Conversion efficiency for positive (closed circles) and negative (open circles) detunings in the quantum-dot and bulk SOAs

7. Precise Measurement of Timing Jitters of Repetitive Laser Pulses

Generation of highly repetitive laser pulses is an important issue for such applications as optical time-division multiplexed (OTDM) communication [62], high-resolution photonic analog-to-digital conversion [63,64], and high-speed optical sampling measurement [65]. Since these applications require stringent performances on pulse timing jitter as well as on pulse width, it has become a matter of great concern to precisely evaluate the magnitude of timing jitter in repetitive laser pulses. For example, to ensure the bit error rate below 10^{-12} in OTDM transmission systems, timing jitter should be less than 1/14.1 of the bit period [66], which corresponds to 443 fs in a 160-Gbit/s transmission.

A commonly employed method for timing jitter measurement is the so-called single sideband (SSB) phase noise measurement proposed by von der Linde [67], which performs noise measurement in a frequency domain and is based on the standard technique used for microwave and millimeter-wave phase noise measurements. If we detect the intensity of repetitive laser pulses with a fast photodiode, the first harmonic component of the electrical output signal is given by

$$I(t) = I_0\{1 + \epsilon(t)\}\sin\{2\pi f_{\mathrm{rep}}t + \phi(t)\}, \tag{2}$$

where I_0 and f_{rep} are the nominal amplitude and repetition frequency, respectively, and $\epsilon(t)$ and $\phi(t)$ represent the amplitude and phase noise, respectively. Timing noise $J(t)$ is related to phase noise $\phi(t)$ by

$$J(t) = \phi(t)/2\pi f_{\mathrm{rep}}. \tag{3}$$

The most fundamental measure of the timing noise is a phase power spectral density (PN-PSD) $S_\phi(f)$ of $\phi(t)$, where f represents the Fourier frequency, and a root-mean-square (RMS) timing jitter σ_J is calculated from $S_\phi(f)$ using the relation

$$\sigma_J(f_h, f_l) = \frac{1}{2\pi f_{\text{rep}}} \sqrt{\int_{f_l}^{f_h} S_\phi(f) df}, \tag{4}$$

where f_l and f_h denote the lower and upper limits of integration, respectively.

In SSB phase noise measurement, the quantity $L(f)$, which is the ratio of the noise power in one sideband to the total signal power, is used as a measure of timing noise. This quantity corresponds to the power spectral density of the first harmonic $I(t)$ and contains information on both the amplitude and phase noise. When the RMS phase deviation is much smaller than 1 radian, $L(f)$ is related to the phase noise power spectral density (PSD) $S_\phi(f)$ by an approximated relation $S_\phi(f) \approx 2L(f)$. Although SSB phase noise measurement is quit easy to implement, it is accompanied by inherent limitations, such as limited frequency span and dynamic range, difficulty in discriminating amplitude and phase noise, and inaccuracy when applied to a non-stationary process such as passively mode-locked laser pulses [68].

In order to overcome the above difficulties, the time domain demodulation (TDD) [69] and the time interval analysis (TIA) [70] techniques were developed, both of which perform measurements in a time domain. The TDD technique directly measures the phase noise $\phi(t)$ of a sinusoidal signal from the in- and quadrature-phase amplitudes, while the TIA technique measures the period $\Delta T = 2\pi\{d\phi(t)/dt\}^{-1}$ using zero-dead-time counters. The former technique offers a high sensitivity but is not suitable for measuring signals exhibiting a timing drift. In contrast, although the sensitivity is limited, the latter technique is effective for the measurement of drifting signals. These two techniques are complementary with each other and are used properly or combined depending on the properties of timing noise.

Since the time domain measurement equipment cannot directly handle highly repetitive signals beyond 10 GHz, electrical and/or optical frequency down conversion is required before signal processing. A double-balanced mixer (DBM) can be employed to down-convert an electrical signal at f_{rep} into a lower frequency IF signal at $f_{\text{IF}} = f_{\text{rep}} - f_{\text{LO}}$, where f_{LO} represents the frequency of an electrical local oscillator (LO). This method is applicable to pulses with the repetition frequency up to 50 GHz [71] as limited by the response time of photodetectors. To down-convert pulses beyond 50 GHz, an optoelectronic harmonic mixer (OEHM) were developed [72] which produces an IF signal at $f_{\text{IF}} = f_{\text{rep}} - nf_{\text{LO}}$ with the help an electro-optic intensity modulator, where n is the integer. The modulator driven by an LO signal generates modulation sidebands located at $\pm nf_{\text{LO}}$ from each longitudinal mode and produces beat signals between the nth sidebands and the adjacent longitudinal modes.

Figure 24 shows the results of timing noise measurement for various repetitive laser pulses, where curves A–E represent the PN-PSD $S_\phi(f)$ and curves F–J represent RMS jitter σ_J. The value of σ_J is calculated for $f_h = 18$ MHz and is plotted as a function of f_l. Curves B and G represent the noise of 19.444 GHz pulses emitted by a hybrid mode-locked laser diode [73] and were evaluated by the combination of TDD and DBM. For comparison, noise of the frequency synthesizer is plotted by curves A and F. Curves A and B almost overlap below 100 kHz Fourier frequency, which suggest that the laser is accurately synchronized with the RF signal. However, the existence of a white noise component above 100 kHz indicates the incomplete synchronization caused by the spontaneous emission coupled into the lasing modes. The RMS jitter for the laser pulses amounts to 3.4 ps (2.5 mHz–18 MHz).

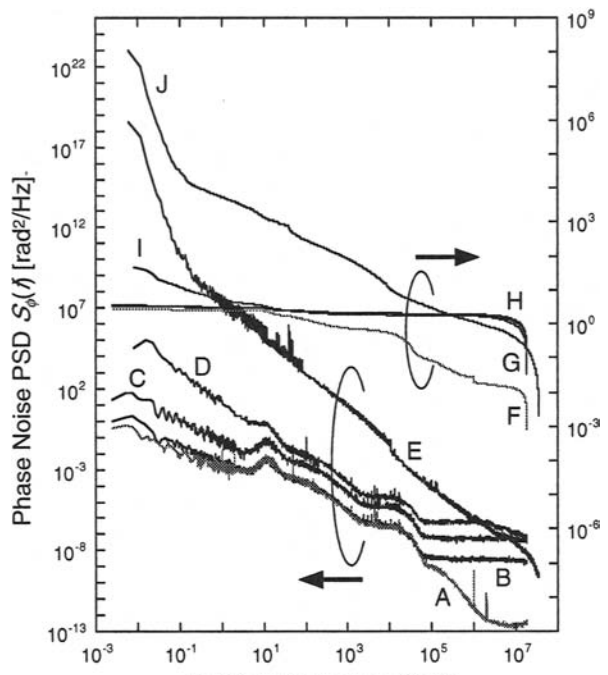

Fig. 24. PN-PSD $S_\phi(f)$ (curves A– E) and RMS timing jitter σ_J. (curves F–J) for various repetitive laser pulses. A, F: frequency synthesizer that drives the 19.444-GHz hybrid mode-locked laser; B, G: 19.444 GHz pulses emitted by hybrid mode-locked laser; C, H: 77.776 GHz OTDM pulses generated from the hybrid mode-locked laser diode; D, I: 155.552 GHz OTDM pulses generated from the hybrid mode-locked laser diode; E, J: 160.64 GHz pulses emitted by the colliding-pulse mode-locked laser diode.

Curves C and H correspond to 77.776 GHz OTDM pulses and were evaluated by the combination of TDD and OEHM. These pulses were generated from the 19.444-GHz mode-locked laser diode by the use of fiber-optic multiplexers. Frequency down-conversion was achieved with the second order modulation sidebands produced by a 40-GHz intensity modulator. The values of $S_\phi(f)$ for curve C are approximately 16 times as large as those on curve B, which is consistent with the increased repetition frequency. Moreover, the shapes of curves B and C are almost identical indicating that the excess noise added during the multiplexing process is small and that the timing noise of the original laser pulses is dominant. The RMS jitter for the OTDM pulses amounts to 3.7 ps, which is almost equal to that of the original laser pulses.

Curves D and I correspond to 155.552 GHz OTDM pulses evaluated by the combination of TDD and OEHM. Although the values of $S_\phi(f)$ on curve D are nearly 64 times as large as those on curve B between 10 Hz and 1 MHz, they increase rapidly below 10 Hz. The observed increase in the low frequency noise is attributed to the thermal drift of the OTDM multiplexer. A slight decrease of $S_\phi(f)$ on curve D above 1

MHz is due to the incoherent addition of the pulse intensity at the output of the OTDM multiplexer [74]. The RMS jitter amounts to 4.5 ps (7.8 mHz–18 MHz).

Curves E and J represent the noise of 160.64 GHz pulses emitted directly by a colliding-pulse mode-locked laser diode [75]. Since the laser exhibits large timing variation under passively mode-locked operation, TIA technique combined with OEHM was employed. The values of $S_\phi(f)$ on curve E are inversely proportional to f^2 above 1 Hz, which is characteristic of random walk noise. However, it rapidly increases below 1 Hz due to the slow drift caused mainly by the temperature variation. The RMS jitter amounts to 0.11 ms (5.8 mHz–34 MHz).

From the above results it can be seen that TDD and TIA techniques have enabled the timing noise evaluation of repetitive laser pulses up to 160 GHz over nine decades of Fourier frequency (2.5 mHz–34 MHz) with 300-dB dynamic range. To handle higher repetitive pulses, nonlinear frequency conversion technique [75] will be promising although it requires a stable reference pulses instead of an electrical LO source.

8. Summary

It is remarkable that many leading research results on the ultrafast optical devices and related technology have been produced in the systematic and long-term R&D of FST project. A novel technology platform of optical devices will be formed by the development of devices in the project.

Using a mode-locked semiconductor laser and SMZ switches developed in the FST project, we successfully accomplished an unrepeated 140 km transmission of 8 $\times$ 160 Gb/s OTDM/DWDM signals [76]. It is also expected that the application of the OTDM technology will be realistically promoted by taking advantage of these advanced devices.

This direction of the R&D will, moreover, open the possibility of the future ultrafast optical signal processing. Ubiquitous information networking system based on such ultrafast optical signal processing and communication technology will play an important role to meet the demands in the business, social security and human life as a flexible and reliable communication system in the future.

Acknowledgments

The authors would like to express their thanks to Profs. and Drs. Masahiro Okabe (section 1), Yoh Ogawa (2), Kiyoshi Asakawa (3), Kazuhito Tajima (3), Ryoichi Akimoto (4), Hiroshi Ishikawa(4), Nobuo Suzuki (4), Makoto Furuki (5), Hajime Imai (6), Hidemi Tsuchida (7), Toshifumi Hasama (8) and Masanobu Watanabe (8) for their contribution of the discussion and paper manuscript.

References

1. Y. Lee, Appl. Phys. Lett., **73**, 2715 (1998).
2. S. Wakabayashi, A. Baba, and H. Moriya, OFC2003, MF27, **1**, 30 (2003).

3. K. Akiyama, N. Tomita, T. Nishimura, Y. Nomura, and T. Isu, 10th Intern. Workshop on Femtosecond Technology, WD-2, 41 (2003).
4. K. Ogawa and M.D. Pelusi, Opt. Comm., 198, 83 (2001).
5. S. Arahira, Y. Matsui, and Y. Ogawa, IEEE J. Quantum Electron., **32**, 1211 (1996).
6. S. Arahira and Y. Ogawa, Electron. Lett., **31**, 808 (1995).
7. Y. K. Chen and M. C. Wu, IEEE J. Quantum Electron., **28**, 2176 (1992).
8. S. Arahira and Y. Ogawa, IEEE Photon. Technol. Lett., **8**, 191 (1996).
9. X. Wang, H. Yokoyama, and T. Shimizu, IEEE Photon. Technol. Lett., **8**, 617 (1996).
10. S. Arahira, Y. Katoh, D. Kunimatsu, and Y. Ogawa, IEICE Trans. Electron., E83-C, 966 (2000).
11. K. Tajima: Jpn. J. Appl. Phys., **32**, L1746 (1993).
12. S. Nakamura, K. Tajima, and Y. Sugimoto, Appl. Phys. Lett., **65**, 283 (1994).
13. K. Tajima, S. Nakamura, and Y. Sugimoto, Appl. Phys. Lett., **67**, 3709 (1995).
14. Y. Ueno, S. Nakamura, K. Tajima, and S. Kitamura, IEEE Photonics Technol. Lett., **10**, 346 (1998).
15. K. Tajima, S. Nakamura, Y. Ueno, J. Sasaki, T. Sugimoto, T. Kato, T. Shimoda, M. Itoh, H. Hatakeyama, T. Tamanuki, and T. Sasaki, IEE Electron. Lett., **35**, 2030 (1999).
16. S. Nakamura, Y. Ueno, K. Tajima, J. Sasaki, T. Sugimoto, T. Kato, T. Shimoda, M. Itoh, H. Hatakeyama, T. Tamanuki, and T. Sasaki, IEEE Photon. Technol. Lett., **12**, 425 (2000).
17. R. Hess, M. Caraccia-Gross, W. Vogt, E. Gamper, P. A. Besse, M. Duelk, E. Gini, H. Melchior, B. Mikkelsen, M. Vaa, K. S. Jepsen, K. E. Stubkjaer, and S. Bouchoule,: IEEE Photon. Technol. Lett., **10**, 165 (1998).
18. S. Nakamura, Y. Ueno, and K. Tajima, Appl. Phys. Lett., **78**, 3929 (2001).
19. Y. Sugimoto, N. Ikeda , N. Carlsson, K. Asakawa, N. Kawai, and K. Inoue, J. App. Phys., **91**, 992 (2002).
20. Y. Sugimoto, N. Ikeda , N. Carlsson, K. Asakawa, N. Kawai, and K. Inoue, Appl. Phys. Lett., **79**, 4286 (2001).
21. Y. Sugimoto, N. Ikeda , N. Carlsson, K. Asakawa, N. Kawai, and K. Inoue, J. Appl. Phys., **91**, 3477 (2002).
22. K. Inoue, T. Maruyama, K. Miyashita, K. Ishida, Y. Sugimoto, N. Ikeda, Y. Tanaka and K. Asakawa: accepted for Jpn. J. Appl. Phys.
23. Y. Sugimoto, Y. Tanaka, N. Ikeda, T. Yang, H. Nakamura, K. Asakawa, K. Inoue, T. Maruyama, K. Miyashita, and K. Ishida, Appl. Phys. Lett., **83**, 3236 (2003).
24. H. Nakamura, S. Nishikawa, S. Kohmoto and K. Asakawa, Proceedings of LEOS2001, San Diego, Wu2 (2001).
25. Y. Sugimoto, Y. Tanaka, N. Ikeda, H. Nakamura, K. Asakawa, and K. Inoue, to be published in the Proceedings of PECS-V, Kyoto, 2004.
26. K. Inoue, N. Kawai, Y. Sugimoto, N. Carlsson, N. Ikeda, and K. Asakawa, Phys. Rev. B, **65**, 121308 (2002).
27. Y. Tanaka, Y. Sugimoto, N. Ikeda, H. Tanaka, K. Asakawa, K. Inoue, and S. Johnson, accepted for Electron. Lett.
28. Y. Sugimoto, Y. Tanaka, N. Ikeda, Y. Nakamura, K. Asakawa, submitted to Opt. Express.

29. K. Kanamoto, H. Nakamura, Y. Nakamura, Y. Sugimoto, N. Ikeda, Y. Tanaka, S. Ohkouchi, H. Ishikawa and K. Asakawa, 2003 IEEE LEOS Annual Meeting Conference Proceedings, 2, 561 (2993).
30. Y. Ueno, S. Nakamura, and K. Tajima, IEEE Photon. Technol. Lett., **13**, 469 (2001).
31. S. Nakamura, Y. Ueno, and K. Tajima, IEEE Photon. Technol. Lett., **13**, 1091 (2001).
32. S. Noda, T. Yamamoto, M. Ohya, Y. Muramoto, and A. Sasaki, IEEE J. Quantum Electron., **29**, 1640 (1993).
33. N. Suzuki, and N. Iizuka, Jpn. J. Appl. Phys., **36**, Pt.2, L1006 (1997).
34. N. Iizuka, K. Kaneko, N. Suzuki, T. Asano, S. Noda, and O. Wada, Appl. Phys. Lett., **77**, 648 (2000).
35. N. Iizuka, K. Kaneko, and N. Suzuki, Appl. Phys. Lett., **81**, 1803 (2002).
36. C. Gmachl, H. M. Ng, and Y. Cho, Appl. Phys. Lett., **79**, 1590 (2001).
37. K. Kishino, A. Kikuchi, H. Kanazawa, and T. Tachibana, Appl. Phys. Lett., **81**, 1234 (2002).
38. T. Mozume, N. Georgiev, T. Simoyama, A. V. Gopal, and H. Yoshida, 14th Indium Phosphide and Related Materials Conf. Stockholm, 2002, Post Deadline Paper.
39. T. Simoyama, H. Yoshida, J. Kasai, T. Mozume, A. V. Gopal., and H. Ishikawa, IEEE Photonic Technol. Lett., **15**, 1363 (2003).
40. H. Yoshida, T. Mozume, A. Neogi, and O. Wada, Electron. Lett., **35**, 1103 (1999).
41. R. Akimoto, Y. Kinpara, K. Akita, F. Sasaki, and S. Kobayashi, Appl. Phys. Lett., **78**, 580 (2001).
42. R. Akimoto, K. Akita, F. Sasaki, and T. Hazama, Appl. Phys. Lett., **81**, 2998 (2002).
43. K. Ridley, Phys. Rev. B, **39**, 5282 (1989)
44. S. Kobayashi and F. Sasaki, J. Lumin. **58**, 113 (1994).
45. K. Minoshima, M. Taiji, K. Misawa, and T. Kobayashi, Chem. Phys. Lett. **218**, 67 (1994).
46. M. Furuki, M. Tian, Y. Sato, L. S. Pu, S. Tatsuura, and O. Wada, Appl. Pys. Lett. **77**, 472 (2000).
47. F. Salin, P. Georeges, G. Roger, and A. Brun, Appl. Opt. **26**, 4528 (1987).
48. D. J. Kane and R. Trebino, Opt. Lett. **18**, 823 (1993).
49. S. Tatsuura, M. Tian, M. Furuki, Y. Sato, L. S. Pu, and O. Wada, Jpn. J. Appl. Phys. **39**, part 1, 4782 (2000).
50. M. Furuki, M. Tian, Y. Sato, L. S. Pu, H. Kawashima, S. Tastuura, and O. Wada, Appl. Phys. Lett. **78**, 2634 (2001).
51. M. Tian, S. Tatsuura, M. Furuki, Y. Sato, I. Iwasa, and L. S. Pu, J. Am. Chem. Soc. **125**, 348 (2003).
52. Y. Sato, M. Furuki, M. Tian, L. S. Pu, and S. Tatsuura, Appl. Phys. Lett. **80**, 2254 (2002).
53. H. Nakajima and R. Fery, Appl. Phys. Lett., **47**, 769(1985).
54. S. Murata, A. Tomita, J. Shimizu, M. Kitamura, and A. Suzuki, Appl. Phys. Lett., **58**, 1458(1991).
55. R. Hui, S. Benedetto, and I. Montrosset, J. Lightwave Technol., **11**, 2026 (1993).
56. H. Kuwatsuka, H. Shoji, M. Matsuda, and H. Ishikawa, Electron. Lett., **31**, 2108 (1995).
57. H. Kuwatsuka, T. Akiyama, B. E. Little, T. Simoyama, and H. Ishikawa, Tech. Digest of 26th European Conference on Optical Communication (ECOC 2000), Vol.3, 65, 2000, Munich.

58. K. Kikuchi, M. Kakui, C-E Zah, and T-P Lee, IEEE Journal of Quantum Electron., **28**, 151 (1992).
59. G. P. Agrawal and N. Andes Olsson, IEEE Journal of Quantum Electron., **25**, 2297 (1989).
60. M. Sugawara, T. Akiyama, N. Hatori, Y. Nakata, K, Otsubo, and H. Ebe, APOC 02, Materials and Devices for Optical and Wireless Communications, Shanghai, in Proceedings of SPIE Vol. 4905, (2002), p. 259.
61. T. Akiyama, H. Kuwatsuka, N. Hatori, Y. Nakata, H. Ebe, and M. Sugawara, IEEE Photon. Tech. Lett., **14**, 1133 (2002).
62. M. Nakazawa, T. Yamamoto, and K. R. Tamura, Electron. Lett., **36**, 2027 (2000).
63. C. M. DePriest, T. Yilmaz, A. Braun, J. Abeles, and P. J. Delfyett, Jr., IEEE J. Quantum Electron., **38**, 380 (2002).
64. A. S. Bhushan, P. V. Kelkar, B. Jalali, O. Boyraz, and M. Islam, IEEE Photon. Technol. Lett., **14**, 684 (2002).
65. M. Shirane, Y. Hashimoto, H. Yamada, and H. Yokoyama, IEEE Photon. Technol. Lett., **12**, 1537 (2000).
66. M. Jinno, IEEE J. Quantum Electron., **30**, 2842 (1994).
67. D. von der Linde, Appl. Phys. B, **39**, 201 (1986).
68. H. A. Haus and A. Mecozzi, IEEE J. Quantum Electron., **29**, 983 (1993).
69. H. Tsuchida, Opt. Lett., **23**, 286 (1998).
70. H. Tsuchida, Opt. Lett., **24**, 1434 (1999).
71. H. Tsuchida, IEEE Photon. Technol. Lett., **14**, 535 (2002).
72. H. Tsuchida, Opt. Lett., **27**, 2040 (2002).
73. S. Arahira, Y. Katoh, and Y. Ogawa, Electron. Lett., **36**, 454 (2000).
74. H. Tsuchida, IEEE J. Sell. Top. Quantum Electron., **9**, 535 (2003).
75. S. Arahira, Y. Katoh, D. Kunimatsu, and Y. Ogawa, IEICE Trans. Electron., **83-C**, 966 (2000).
76. A. Suzuki, X. Wang, T. Hasegawa, Y. Ogawa, S. Arahira, K. Tajima, and S. Nakamura, ECOC 2003, Mo3.6.1, 1, 44 (2003).